

Crop classification from full-year fully-polarimetric L-band UAVSAR time-series using the Random Forest algorithm

Huapeng Li^{a,b,*}, Ce Zhang^{b,c,**}, Shuqing Zhang^a, Peter M. Atkinson^d

^a Northeast Institute of Geography and Agroecology, Chinese Academy of Sciences, Changchun 130012, China

^b Lancaster Environment Centre, Lancaster University, Lancaster LA1 4YQ, UK

^c Centre for Ecology & Hydrology, Library Avenue, Bailrigg, Lancaster LA1 4AP, UK

^d Faculty of Science and Technology, Lancaster University, Lancaster LA1 4YR, UK

ARTICLE INFO

Keywords:

Crop classification
Multitemporal SAR imagery
Polarimetric SAR
Random Forest algorithm
UAVSAR

ABSTRACT

Accurate and timely information on the distribution of crop types is vital to agricultural management, ecosystem services valuation and food security assessment. Synthetic Aperture Radar (SAR) systems have become increasingly popular in the field of crop monitoring and classification. However, the potential of time-series polarimetric SAR data has not been explored extensively, with several open scientific questions (e.g. the optimal combination of image dates for crop classification) that need to be answered. In this research, the usefulness of full year (both 2011 and 2014) L-band fully-polarimetric Uninhabited Aerial Vehicle Synthetic Aperture Radar (UAVSAR) data in crop classification was fully investigated over an agricultural region with a heterogeneous distribution of crop categories. In total, 11 crop classes including tree crops (almond and walnut), forage crops (grass, alfalfa, hay, and clover), a spring crop (winter wheat), and summer crops (corn, sunflower, tomato, and pepper), were discriminated using the Random Forest (RF) algorithm. The SAR input variables included raw linear polarization channels as well as polarimetric parameters derived from Cloude-Pottier (CP) and Freeman-Durden (FD) decompositions. Results showed clearly that the polarimetric parameters yielded much higher classification accuracies than linear polarizations. The combined use of all variables (linear polarizations and polarimetric parameters) produced the maximum overall accuracy of 90.50 % and 84.93 % for 2011 and 2014, respectively, with a significant increase of approximately 8 percentage points compared with linear polarizations alone. The variable importance provided by the RF illustrated that the polarimetric parameters had a far greater influence than linear polarizations, with the CP parameters being much more important than the FD parameters. The most important acquisitions were the images dated during the peak biomass stage (July and August) when the differences in structural characteristics between most crops were the largest. At the same time, the images in spring (April and May) and autumn (October) also contributed to the crop classification since they respectively provided unique information for discriminating fruit crops (almond and walnut) as well as summer crops (corn, sunflower, and tomato). As a result, the combined use of only four acquisitions (dated May, July, August, and October for 2011 and April, June, August, and October for 2014) was adequate to achieve a nearly-optimal overall accuracy. In light of the promising classification accuracies demonstrated in this research, it becomes increasingly viable to provide accurate and up-to-date crops inventories over large areas based solely on multitemporal polarimetric SAR.

1. Introduction

Information on crop types and their spatial distribution is of great importance to agricultural management, ecosystem services valuation and food security assessment (Thenkabail et al., 2012; Bargiel, 2017). For example, detailed crop distribution data are critical for assessing

accurately agricultural water use at different spatial scales and making effective policies to increase water use efficiency in agricultural areas (Zheng et al., 2015). Agriculture is also a major source of greenhouse gas (GHG); high accuracy modelling of GHG emissions from agriculture relies heavily on the detailed distribution of crop types (Pena-Barragan et al., 2011). Besides, crop classification data is the fundamental input

* Corresponding author at: Northeast Institute of Geography and Agroecology, Chinese Academy of Sciences, Changchun 130012, China.

** Corresponding author at: Lancaster Environment Centre, Lancaster University, Lancaster LA1 4YQ, UK.

E-mail addresses: lihuapeng@iga.ac.cn (H. Li), c.zhang9@lancaster.ac.uk (C. Zhang).

to estimating agricultural production, which serves as an important early warning indicator of famine (Thornton et al., 1997). As a result, crop maps are updated routinely in many cropland regions by ground survey. However, this procedure is usually labour intensive and expensive, and is impractical for many developing countries. In addition, it is difficult to generate consistent and intercomparable data between countries or even continents in consideration of the different ground field survey methods adopted (Ozdogan and Woodcock, 2006).

Remote sensing, which provides routine coverage over large areas, could serve as a cost-effective means of complementing or even replacing field survey. A large body of studies has classified single or multiple crop types using optical images at medium spatial resolution (e.g. Landsat and SPOT; Duro et al., 2012), or coarse resolution (e.g. MODIS; Wardlow and Egbert, 2008). However, access to optical remotely sensed imagery relies heavily on the weather conditions, which hugely limits the utility of such data in real applications (Sonobe et al., 2014). Synthetic aperture radar (SAR) is an active sensor which operates at relatively long wavelengths and which can penetrate cloud and haze. As a result, SAR provides the best opportunity for monitoring crops through the growing season as it is able to acquire data regardless of meteorological conditions (Sonobe et al., 2014). SAR imagery differs from reflectance measured by optical imagery, as SAR characterizes the structural attributes as well as the dielectric properties of the vegetation canopy which may be unique to each class, thus being valuable for crop discrimination (McNairn et al., 2009).

Different from other land cover types, agricultural regions may experience great variations during a short time depending on climatic conditions, soil properties, farmer's decisions, and so on (Wardlow and Egbert, 2008). Thus, crop areas with the same crop type may have distinctive polarimetric (spectral) properties, whereas those with different crop types often exhibit similar polarimetric behaviours (Li et al., 2019). This poses great difficulties for single-date SAR image-based crop classification (Silva et al., 2009), which can be improved by the utilization of image time series. As a certain crop type might be correctly separated from others at specific crop stages (Jiao et al., 2014; Bargiel, 2017), multi-temporal SAR data can thus improve crop classification results (Skriver et al., 2012). For example, Tso and Mather (1999) classified an agricultural area in Norfolk, UK with seven ERS-1 SAR images, obtaining a classification accuracy of 75 %; with six scenes of ENVISAT ASAR images, Wang et al. (2010) mapped an agricultural area in south China and produced an overall accuracy of 80 %. Recently, some studies attempted to classify crop types using SAR time series from the newly launched Sentinel-1 satellites (e.g. Nguyen et al., 2016; Ndikumana et al., 2018). However, the SAR data used in these works were restricted to single polarization (ERS-1 and Radarsat-1) or dual-polarization mode (ENVISAT ASAR and Sentinel-1), thus without making full use of polarization information.

Radar response to vegetation structure is polarization-dependent. Herein, horizontally polarized waves (H) show good capability in penetrating the vegetation canopy, thus achieving more information about surface soil condition by HH polarization. In contrast, vertically polarized waves are very sensitive to vertical vegetation structure, which explains the fact that VV polarization performs well in characterizing vertical vegetation structure (Lin and Sarabandi, 1999). Moreover, the cross polarizations (HV and VH) provide information about the total canopy volume that is complementary to the co-polarizations (HH and VV). The fully polarimetric SAR, with all types of polarizations, can significantly improve the observed information dimension of agricultural targets (McNairn and Brisco, 2004). In addition, polarimetric parameters that provide unique information for crop discrimination can be generated with full polarimetric (HH, HV, and VV) SAR (Jiao et al., 2014). McNairn et al. (2009) demonstrated the unique value of polarimetric SAR in crop classification in comparison to single- or dual-polarization data. With polarimetric SAR time-series, efforts had been devoted to crop classification. For example, Jiao et al. (2014) achieved promising crop classification results (with overall

accuracy > 90 %) over an agricultural area in Canada with 19 scenes of C-band RADARSAT-2 data; with the same data type, Liu et al. (2013) obtained an overall classification accuracy of 85 % in classifying corn, spring wheat, and soybean over a test site in Eastern Ontario, Canada; Whelen and Siqueira (2017) acquired the best classification accuracy of 83 % on an agricultural site in California's San Joaquin Valley by using L-band Uninhabited Aerial Vehicle Synthetic Aperture Radar (UAVSAR). The above-mentioned classification results are encouraging. However, the full year or full growing season SAR data adopted by these studies are heavily redundant, and such data requirements suffer from high expense, limited data availability, and low data processing efficiency. In contrast, comparable crop classification results might be achieved by combining a few images dated on critical phenology (Jiao et al., 2014; Li et al., 2019). Such research topic has, however, received little attention. In addition, few efforts have been made to quantitatively investigate the importance of polarimetric parameters, although they are widely used in crop classification studies.

The primary objective of this paper was to explore the potential of L-band UAVSAR time-series for crop mapping. With a relatively long wavelength, UAVSAR has the capacity to penetrate crop canopies, which is critical for crop classification. UAVSAR data are acquired in polarimetric mode with fine spatial resolution (5 m) by National Aeronautics and Space Administration (NASA), which provides a unique opportunity to assess the usefulness of multitemporal fully-polarimetric SAR for crop classification. Herein, the Random Forest (RF) classifier, an ensemble machine learning technique, was applied to the UAVSAR time-series in light of its robust to high-dimensional and noise data (Belgiu and Dragut, 2016). Besides, previous studies have demonstrated that the RF algorithm is suitable for SAR-based crop classification (Loosvelt et al., 2012a, 2012b). An agricultural region with heterogeneous and complex crop types in the Sacramento Valley, California was selected as the test site in this research.

The major innovations and contributions of this research are summarized as follows:

- (1) By using the well-known non-parametric machine learning RF algorithm, the potential of different combinations of predictor variables in crop discrimination was fully explored;
- (2) The variable importance for crop classification was quantified across input variables (including linear polarizations and polarimetric parameters) as well as over acquisitions spanning two full calendar years (2011 and 2014);
- (3) A forward selection procedure was conducted to search for the optimal combination of SAR images that made the best tradeoff between classification accuracy and number of acquisitions, which could be transferable to other agricultural areas.

2. Study area and data source

2.1. Study area

The study area of this research is located at an agricultural region in the middle of the Sacramento Valley, USA. It stretches over Solano and Yolo counties of California, with a size of about 11 km × 17 km (Fig. 1). The climate of this area is characterized as Mediterranean, with dry hot summers and wet cool winters (Zhong et al., 2012). The annual rainfall amount is nearly 750 mm, mainly concentrated during the period from winter to the next spring. This area is characterized by a vast flat terrain and deep soil layers which makes it suitable for farming. Indeed, it is one of the most productive agricultural areas in the United States. A total of 11 crop types comprising most of the study area were considered in this research, including almond, walnut, grass, alfalfa, hay, clover, winter wheat, corn, sunflower, tomato and pepper. These multiple crop types provide a unique opportunity to investigate the capability of time-series UAVSAR for crop classification over heterogeneous regions.

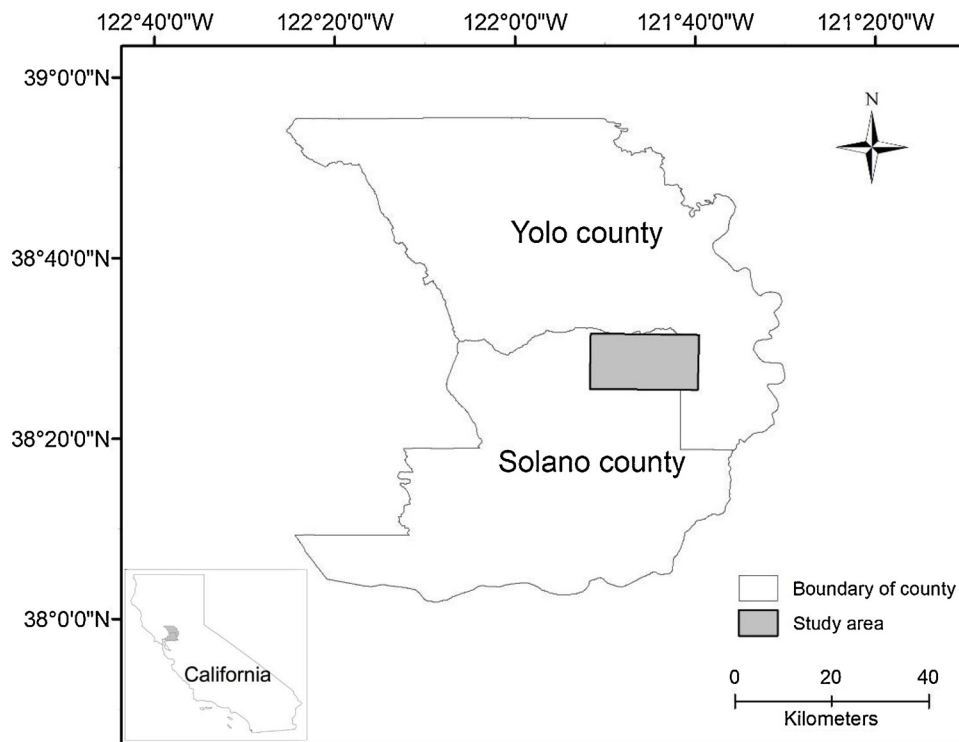


Fig. 1. Location of the study area in the Sacramento Valley, California.

2.2. UAVSAR data

Full-polarimetric airborne UAVSAR data were employed in this research. This SAR system was developed by NASA JPL, with the primary design goal of monitoring deforming surfaces resulting either from natural factors or human activities (Hensley et al., 2009). It operates in L-band with a frequency of 1.26 GHz and a wavelength of 23.84 cm. Nominally, the system flown at an altitude of 12.5 km covers a swath of about 20-km (Chapman et al., 2011), and all flights have nearly identical flight headings and altitude. The range and azimuth pixel spacings in single-look complex (SLC) imagery are, respectively, 1.66 and 1 m, with the incidence angles ranging from 25° to 65°.

The UAVSAR images used in this research were the calibrated and ground range projected (GRD) product. The covariance matrices contained in the product are multilook with 3×12 pixels in the range and azimuth directions, with a pixel spacing of 5 m. The linear polarization channels for each dataset were extracted and georeferenced to the UTM coordinate using the MapReady software (Alaska Satellite Facility, ASF). There was no requirement to apply speckle filters as the multiplicative noise (speckle) inherent in the SAR was reduced markedly by the multilook procedure (Dickinson et al., 2013), producing an estimated equivalent number of looks between 6 and 8. Besides, no further geometric corrections were made in view of the small spatial shifts (lower than half the pixel) across the time-series by checking the boundaries of some randomly selected crop fields. This high-precision spatial matching between acquisitions is essential to classification based on multitemporal UAVSAR.

In total, nine scenes of UAVSAR imagery spanning the full year of 2011 were collected over the study area. Besides, seven scenes of UAVSAR imagery captured in 2014 were also acquired to further investigate the potential of UAVSAR time series for crop classification. Table 1 provides detailed descriptions of the data as well as meteorological data on the image acquisition dates. The meteorological data were acquired at a station (in the city of Sacramento) next to the study area (National Oceanic and Atmospheric Administration and National Centers for Environmental Information (NOAA-NCEI, 2011)). The

Table 1

UAVSAR imagery and the weather conditions at the time of image acquisition. All images were acquired in PolSAR (polarimetric SAR) mode, and there was no snow at the date of acquisition.

Year	Date	Local time	P_{cum} (mm)	T_{max} (°C)	T_{min} (°C)
2011	2011.01.10	20h59	0	8.3	-2.8
	2011.03.30	20h00	0	26.7	11.7
	2011.05.12	22h22	0	26.1	9.4
	2011.06.16	13h04	0	31.1	14.4
	2011.07.20	18h54	0	35.6	15.0
	2011.08.29	20h21	0	34.4	14.4
	2011.10.03	22h02	0.5	20.6	10.0
	2011.11.02	22h45	0	22.8	5.6
	2011.12.07	20h20	0	14.4	-0.6
	2014	2014.02.12	19h15	0	17.8
2014.04.02		19h01	0	16.1	6.1
2014.05.15		18h43	0	36.1	13.9
2014.06.16		18h52	0	24.4	13.3
2014.08.14		22h44	0	32.2	16.1
2014.10.06		20h17	0	35.6	13.9
2014.11.13		21h11	6.6	17.2	12.8

Note that P_{cum} denotes daily precipitation, and T_{max} and T_{min} denote daily maximum and minimum air temperatures, respectively.

presence of rainfall may have an impact on crop classification owing to the higher moisture contained in the canopy and soil. Fortunately, nearly all the UAVSAR images were collected under dry conditions except the acquisition in October 2011 and November 2014 when very light precipitation (less than 7 mm) was recorded (Table 1). Besides, freezing in the soil may also interfere with the radar response by altering the dielectric constant of soil. However, the effect of freezing on the SAR observations should be minimal given the relatively small amounts of precipitation on the data acquisition dates (January and December 2011) with air temperatures around freezing point (Table 1).

3. Methods

In this section, the data preprocessing and analysis methodologies

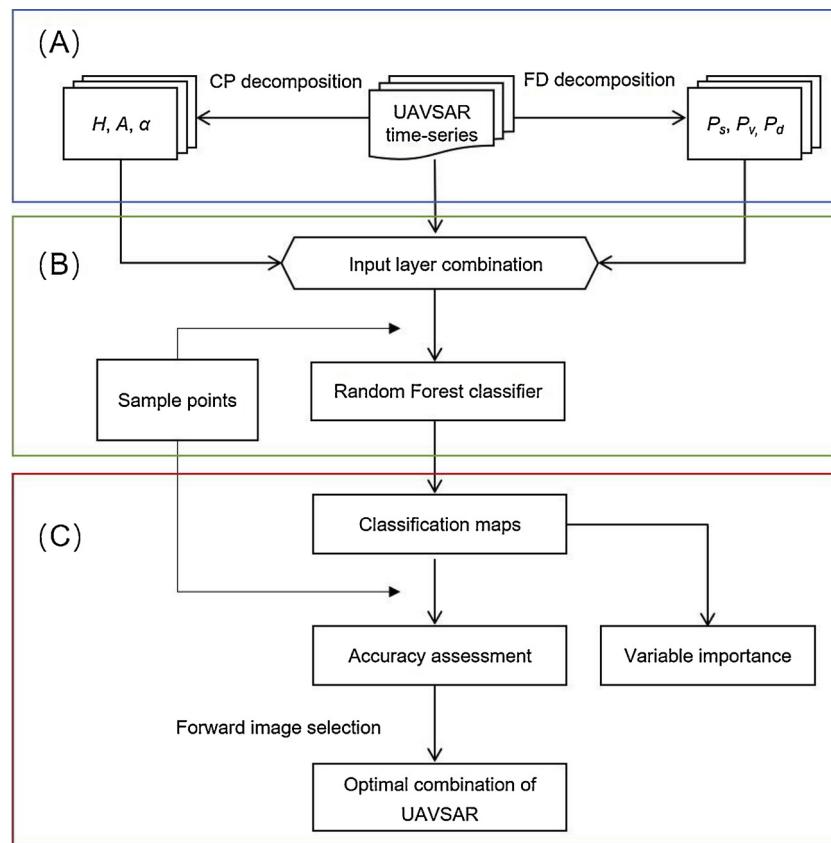


Fig. 2. Flowchart of processing and analysis steps in this work. (A) data pre-processing steps, (B) image classification steps, and (C) analysis steps.

were elaborated in detail. A flowchart that illustrates data processing and analysis steps of this research is shown in Fig. 2.

3.1. SAR polarimetric decomposition

The rationale for a decomposition lies in the fact that polarimetric SAR signal can be deconstructed to derive polarimetric parameters that characterize structural properties and the scattering mechanisms of ground targets. In this research, two widely accepted decompositions, Cloude-Pottier (CP) and Freeman-Durden (FD), were applied to each UAVSAR dataset. The former is an eigenvector-eigenvalue based decomposition, while the latter belongs to the family of model-based decompositions. The CP decomposition is designed to characterize primary scattering mechanisms for surface targets (Cloude and Pottier, 1997), with three parameters including entropy (H), anisotropy (A), and alpha angle (α) being commonly generated. Both entropy and anisotropy vary between 0–1, while alpha angle has a range of 0–90°. Entropy is a measurement of the randomness of scattering, with a high value indicating a multiplicity of scattering mechanisms. Anisotropy describes the relative importance of the secondary mechanism, and the value represents the strength of scattering. Alpha angle characterizes the dominant scattering mechanisms, with angle values below 40°, around 45°, and over 50° denoting the dominance of surface scattering, volume or dipole scattering, and double-bounce scattering, respectively. The FD decomposition is built on a physical model, based on which fractions of surface scattering (P_s), volume scattering (P_v), and double-bounce scattering (P_d) are determined for each target (each pixel of image) (Lee and Pottier, 2009). The model describes the polarimetric backscatter from natural scatterers including first-order Bragg surface, double-bounce dihedral corner reflector, and thin randomly oriented cylindrical dipoles (Freeman and Durden, 1998).

3.2. Collection of reference data

The United States Department of Agriculture (USDA) Cropland Data Layer (CDL) served as the reference data to acquire ground samples for crop classification and validation. The CDL is produced annually based on several types of medium spatial resolution optical images (e.g. Landsat TM) and a large number of ground reference data (Boryan et al., 2011), with a spatial resolution of 30 m. CDL data have been used in a wide range of applications because of its very high quality (e.g. Sun et al., 2008; Zheng et al., 2015; Whelen and Siqueira, 2017). According to the USDA National Agricultural Statistics Services (NASS), the overall classification accuracy for the CDL in 2011 and 2014 over the state of California was determined to be 83 % and 81 %, respectively, with the accuracies for the major crop types (alfalfa, sunflower, and tomato) ranging between 83 % and 94 %. It is noted that the mislabeled pixels of CDL are mainly at the edge of crop fields and the fields with relatively small area by visual inspection. However, these areas were not included in the subsequent manual labelling procedure (see below), by which the actual accuracies of the reference data used in this research should be much higher than those reported by the USDA-NASS.

The acquisition of ground sample points was comprised of three steps. First, the August SAR acquisition with clear boundaries between crop fields was overlaid on the CDL image to identify crop fields over the study area; note that fields with an area below 5 ha were not considered. Second, the identified crop fields were outlined manually and buffered inward by one pixel to remove the mislabeled edge pixels (Fig. 3); a stratum for each crop class was made by merging the outlined patches belonging to the class. Third, patches of each crop type were split randomly into two equal subsets; one half subset was for generating training samples, and the other half subset for collecting testing samples, so as to make sure that training and testing samples are taken from different crop patches. In total, 2316 and 2124 sample points (pixels) were acquired for 2011 and 2014, respectively, with a number

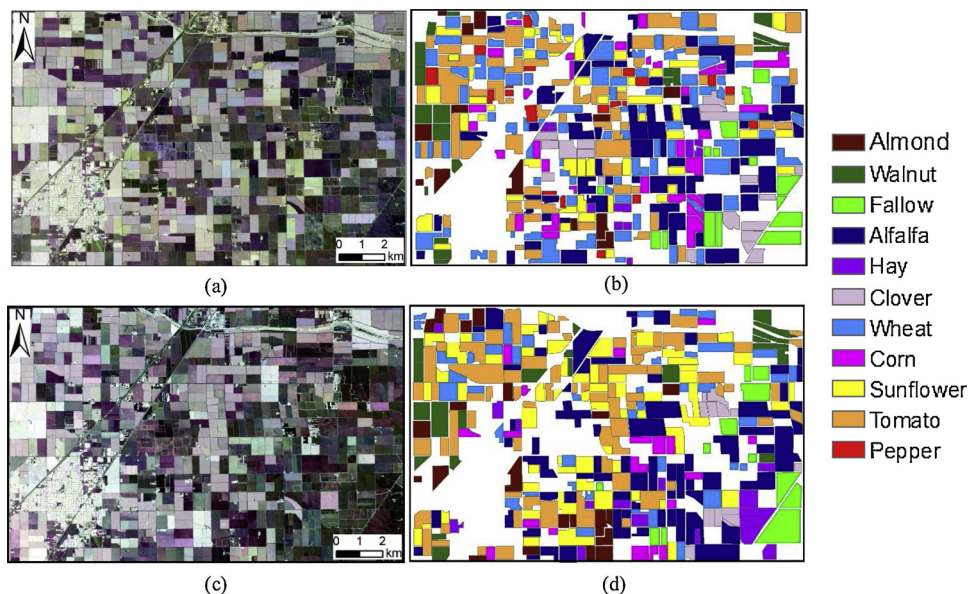


Fig. 3. False colour map of the UAVSAR dated on 20 July 2011 (bands VV, HV, HH) (left), and the manually labeled ground reference data (right).

of about 200 samples for each crop type.

3.3. Random Forest classification

In total, nine predictor variables were created from each UAVSAR dataset, consisting of three linear polarizations (HH, HV and VV), three CP decomposition parameters (H , A and α), and three FD decomposition parameters (P_s , P_v , P_d). The Random Forest (RF) algorithm was applied using different combinations of input image layers: 1) linear polarizations alone, 2) CP decomposition parameters alone, 3) FD decomposition parameters alone, and 4) all predictor variables (linear polarizations and CP and FD parameters). Descriptions of the combinations of input variables are shown in Table 2.

The RF algorithm is an ensemble classifier consisting of a collection of tree-type classifiers $\{h(x, \theta_k), k = 1, 2, \dots, T\}$, where x is an input vector (pattern), θ_k are independent and identically distributed random vectors, and T is the number of trees defined by users (Breiman, 2001). In the training process, the RF creates multiple classification and regression trees, each of which is trained on a different bootstrap sample by randomly resampling the original training sample with replacement (called bagging strategy). For an input pattern x each tree votes for the predicted class and the pattern is labelled with the class having the most votes. In this research, the number of trees created for each classification was set as 500 to achieve a stable state for the out-of-bag (OOB)

Table 2
Summary of predictor variables derived from UAVSAR for RF classification. Note that abbreviations are explained in the text.

Year	Data source	Variable	Number of Images	Number of layers
2011	LP	HH, HV, VV	9	9×3 = 27
	CP	H , A , α	9	9×3 = 27
	FD	P_s , P_v , P_d	9	9×3 = 27
	All	HH, HV, VV, H , A , α , P_s , P_v , P_d	9	9×9 = 81
2014	LP	HH, HV, VV	7	7×3 = 21
	CP	H , A , α	7	7×3 = 21
	FD	P_s , P_v , P_d	7	7×3 = 21
	All	HH, HV, VV, H , A , α , P_s , P_v , P_d	7	7×9 = 63

accuracy of the RF. Besides, the square root of inputs was used as the number of variables to determine splits at the nodes.

The variable importance (VI) provided by the RF can not only quantify the influence of each variable separately, but also multivariate interactions with other variables (Gislason et al., 2006). In general, the VI for a certain variable X_i can be estimated with the following steps. First, the prediction error with OOB samples (err_{OOB}) is calculated over the created trees. Second, the classifier randomly permutes the OOB samples of variable X_i , with which the prediction error (err_{OOB}^i) for each tree is measured. Finally, the VI is computed by averaging the difference in the prediction errors between original OOB samples and randomly permuted samples through all trees as follows:

$$VI(X^i) = \frac{1}{ntree} \sum_{t=1}^{ntree} err_{OOB}_t^i - err_{OOB}_t \quad (1)$$

where t denotes a certain tree, and $ntree$ is the total number of trees. The VI is subsequently normalized by dividing the variable's VI by its standard deviation.

3.4. Accuracy assessment

To evaluate the accuracies of the classification maps, a confusion matrix was generated for each classification by comparing the classified data with the reference points at each of the sampled pixels. The overall accuracy (OA) and per-class mapping accuracy were computed for each classification (Foody, 2004). The Kappa coefficients of agreement and their variances were also estimated, based on which a Kappa z-test was adopted to evaluate the statistical significance of Kappa coefficients for pairwise classifications using the following equation (Congalton and Green, 1999):

$$z = (k_1 - k_2) / \sqrt{(v_1 + v_2)} \quad (2)$$

where k is the Kappa coefficient and v is the Kappa variance. If z exceeds a threshold of 1.96, the two classification results are considered significantly different at the 95 % confidence level.

3.5. Optimal combination of SAR data

In total, nine scenes of images in 2011 and seven scenes of images in 2014 covering a full calendar year respectively were used in this research. However, contributions from different acquisitions to crop

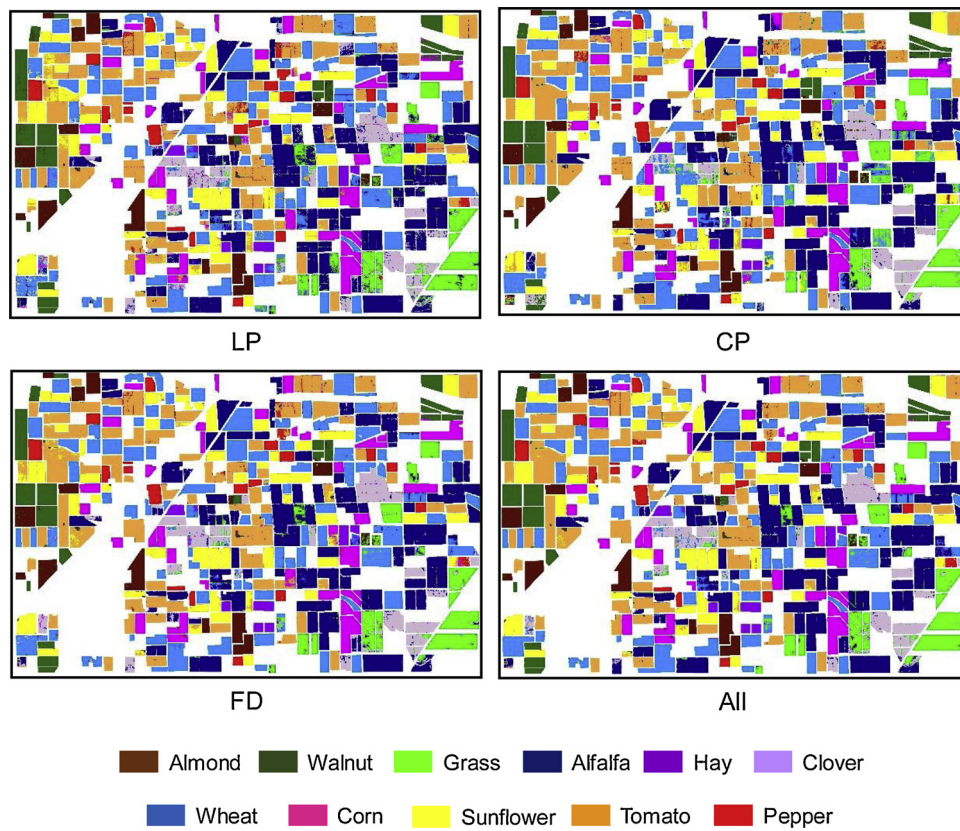


Fig. 4. Crop classification maps of 2011 produced with the Random Forest algorithm using the linear polarizations (LP), Cloude-Pottier parameters (CP), Freeman-Durden parameters (FD), and all predictor variables (All).

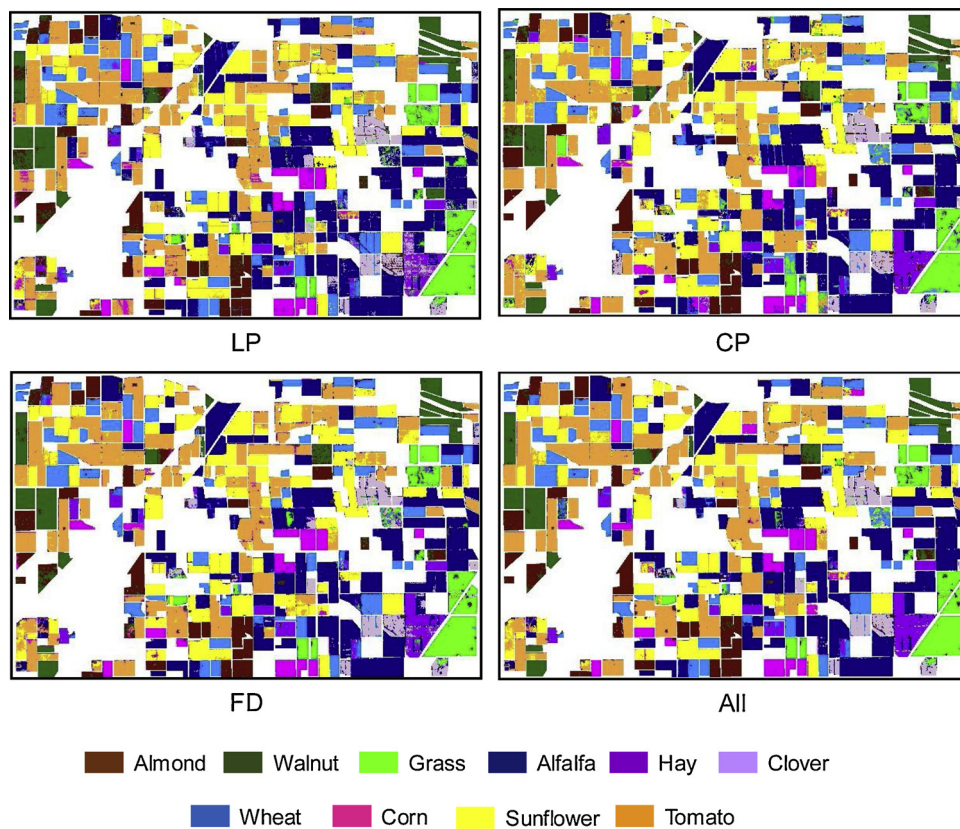


Fig. 5. Crop classification maps in 2014 produced with the Random Forest algorithm using the linear polarizations (LP), Cloude-Pottier parameters (CP), Freeman-Durden parameters (FD), and all predictor variables (All).

Table 3

Accuracy assessment of RF classifications (2011) using different combinations of variables. Note that the greatest mapping accuracy (MA) per row is shown in the bold font.

Crop class	LP			CP			FD			All		
	PA	UA	MA	PA	UA	MA	PA	UA	MA	PA	UA	MA
Almond	93.33	93.33	93.33	93.33	95.45	94.38	95.56	95.56	95.56	95.56	95.56	95.56
Walnut	93.48	92.47	92.97	92.39	89.47	90.91	97.83	94.74	96.26	96.74	94.68	95.70
Grass	85.56	74.04	79.38	82.22	77.08	79.57	88.89	85.11	86.96	94.44	81.73	87.63
Alfalfa	73.13	79.67	76.26	88.06	83.69	85.82	85.07	84.44	84.76	89.55	91.60	90.57
Hay	58.23	95.83	72.44	60.76	96.00	74.42	68.35	98.18	80.60	62.03	100	76.56
Clover	71.28	72.04	71.66	61.70	68.24	64.80	77.66	76.04	76.84	78.72	84.09	81.32
Wheat	89.34	76.22	82.26	86.07	66.88	75.27	95.08	83.45	88.89	95.90	80.14	87.31
Corn	82.73	87.50	85.05	93.64	98.10	95.81	90.91	93.46	92.17	99.09	98.20	98.64
Sunflower	78.26	89.11	83.33	77.39	90.82	83.57	79.13	92.86	85.45	86.09	97.06	91.24
Tomato	86.92	71.52	78.47	93.85	84.72	89.05	94.62	78.34	85.71	96.15	87.41	91.58
Pepper	91.18	92.08	91.63	92.16	94.95	93.53	86.27	95.65	90.72	93.14	95.00	94.06
OA	82.38			84.63			87.65			90.50		
Kappa	0.8055			0.8302			0.8636			0.8951		

Table 4

Accuracy assessment of RF classifications (2014) using different combinations of variables. Note that the greatest mapping accuracy (MA) per row is shown in the bold font.

Crop class	LP			CP			FD			All		
	PA	UA	MA	PA	UA	MA	PA	UA	MA	PA	UA	MA
Almond	79.05	78.30	78.67	92.38	76.38	83.62	89.52	76.42	82.46	95.24	83.33	88.89
Walnut	80.58	77.57	79.05	71.84	90.24	80.00	70.87	83.91	76.84	81.55	93.33	87.05
Grass	77.78	82.89	80.25	79.01	75.29	77.11	79.01	87.67	83.12	80.25	90.28	84.97
Alfalfa	79.20	68.75	73.61	85.60	71.81	78.10	83.20	78.79	80.93	86.4	77.14	81.51
Hay	26.83	81.48	40.37	52.44	66.15	58.50	52.44	70.49	60.14	47.56	95.12	63.41
Clover	81.25	64.36	71.82	86.25	86.25	86.25	80.00	70.33	74.85	88.75	78.89	83.53
Wheat	95.20	81.51	87.82	79.20	83.19	81.15	92.80	85.29	88.89	96	79.47	86.96
Corn	60.42	84.06	70.30	66.67	79.01	72.32	68.75	89.19	77.65	82.29	92.94	87.29
Sunflower	75.56	88.70	81.60	80.00	78.26	79.12	82.96	77.78	80.29	87.41	84.29	85.82
Tomato	88.46	67.25	76.41	80.00	76.47	78.20	90.00	82.98	86.35	90.77	88.72	89.73
OA	76.18			78.06			80.32			84.93		
Kappa	0.7336			0.7550			0.7801			0.8316		

Table 5

Kappa z-test comparing the performance of the four RF classifications using different combinations of predictor variables. Note that significantly different accuracies at 95 % confidence level are shown in bold.

Year	Data source	Kappa coefficient (κ)		Kappa z-test		
		Kappa	Variance (10^{-4})	CP	FD	All
2011	LP	0.8055	1.7644	1.3476	3.2990	5.3225
	CP	0.8302	1.5949	-	1.9505	3.9760
	FD	0.8636	1.3372	-	-	2.0305
	All	0.8951	1.0695	-	-	-
2014	LP	0.7336	2.4538	0.9792	2.1633	4.7597
	CP	0.7550	2.3228	-	1.1846	3.7792
	FD	0.7801	2.1665	-	-	2.5906
	All	0.8316	1.7855	-	-	-

classification accuracy may vary greatly (Li et al., 2019). Hence, it is necessary to determine an optimal combination of images that could gain an acceptable level of classification accuracy. This may not only reduce the cost of images, but also lighten the computational burden of image processing and classification. In this research, a forward image selection procedure was adopted in search of the optimal combination of SAR imagery for crop classification (Pena and Brenning, 2015). Hereinto, the images were gradually selected and included in the feature set (starting with an empty feature set) with an increment of one date, and the image combination with the best classification accuracy was chosen at each step.

4. Results

4.1. Random Forest classifications

Figs. 4 and 5 show the classification maps achieved by the Random Forest (RF) algorithm using different combinations of predictor variables from 2011 and 2014 UAVSAR time series, respectively. Tables 3 and 4 list the detailed accuracy assessment of the RF classifications with overall accuracy (OA), Kappa coefficient (κ) as well as class-wise producer's accuracy (PA), user's accuracy (UA), and mapping accuracy (MA, i.e. F1 score). From the tables, it can be seen that the classification based on LP temporal profile has the smallest OAs, 82.38 % and 76.18 % for 2011 and 2014, respectively. By comparison, both CP and FD parameters achieved much more accurate results, with OAs = 83.63 % and 87.65 % for 2011 and OAs = 78.06 % and 80.32 % for 2014, respectively (Tables 3 and 4). When simultaneously using the LP, CP, and FD temporal profiles, the RF produced the highest OAs of 90.50 % and 84.93 % for 2011 and 2014 respectively, which were significantly greater than those using LP, CP, or FD temporal profiles according to the Kappa z-test analysis (Table 5). However, there was no significant difference when comparing the RF classifications with CP parameters and FD parameters.

The classification accuracies amongst classifications were also compared by class-wise accuracy assessment (Tables 3 and 4). As shown in the tables, similar trends are found between the MA and the PA and UA when using different predictor variables. Thus, the MA is taken as an example to analyze variations of the class-wise accuracy. From the tables, it can be seen that the MA produced with all variables

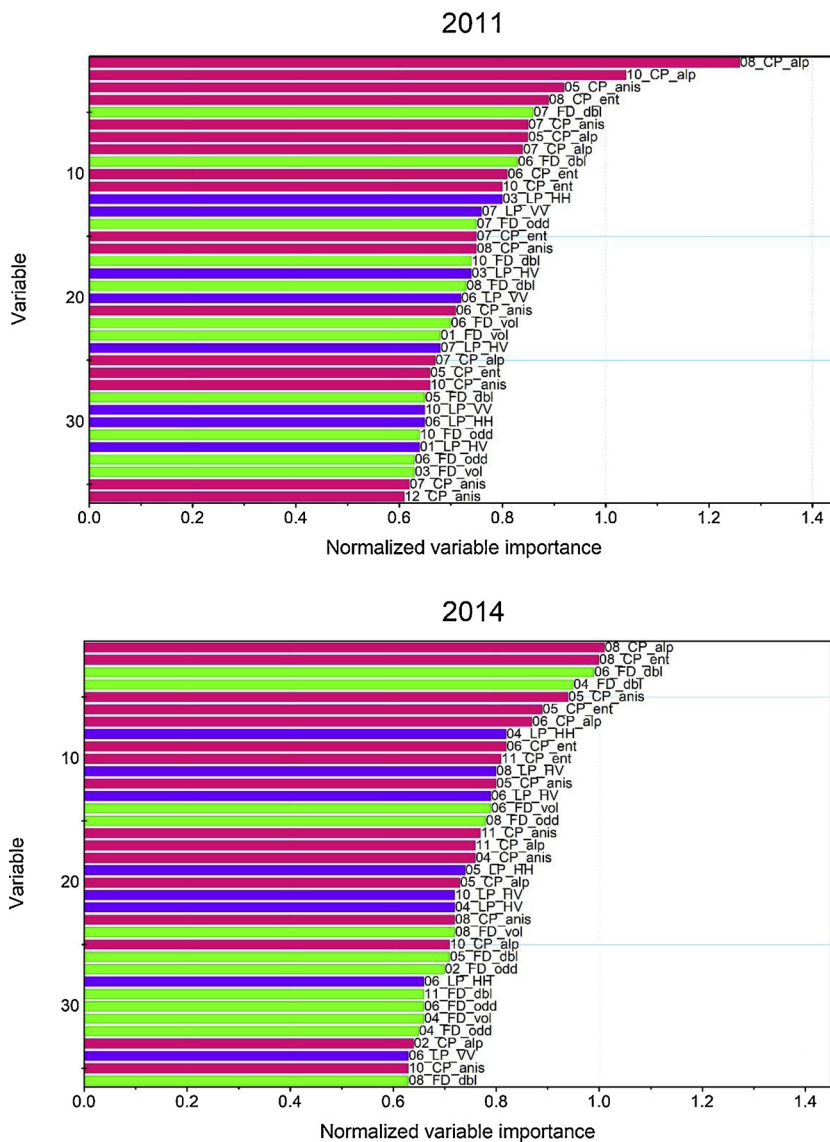


Fig. 6. Normalized variable importance of RF classification using all variables with bars in green, pink, and violet indicating the variables from the linear polarizations, CP decomposition, and FD decomposition, respectively. A variable name consists of three parts, with the prefix, centre, and suffix respectively indicating date of acquisition, data source, and a certain variable (abbreviations ent, anis, alp, odd, vol, and dbl denote the polarimetric parameters of entropy, anisotropy, alpha angle, surface scatter, double-bounce scatter, and volume scatter, respectively). For example, the first variable name 08_CP_alp represents the variable alpha angle derived from the CP decomposition using the August image.

outperforms that based on LP channels for all crop classes in both of the years. Prominent increases in accuracy were seen for the classes of alfalfa, corn, and tomato in 2011, and for those of hay, tomato, and clover in 2014, with a relatively large margin of 14.31, 13.59, and 13.11 percentage points (Table 3), and 23.04, 16.99, and 13.32 percentage points (Table 4), respectively. Similarly, class-wise mapping accuracies with all variables were found to be consistently superior to those with CP parameters, achieving the largest increase of 16.52 and 14.97 percentage points for the classes of clover (2011, Table 3) and corn (2014, Table 4), respectively. When compared with the classification using FD parameters, most classes except for walnut, hay, and wheat in 2011 and wheat in 2014 were classified with greater accuracy, with the largest increase of 6.47 and 10.21 percentage points for corn (2011) and walnut (2014), respectively.

4.2. Variable importance

The RF classifications with all variables were selected to investigate the relative importance of input variables for crop classification. Among the 81 variables used by the RF, the most important 36 variables are listed in descending order in Fig. 6. It is clear from the figure that the variables derived from the CP decomposition are generally important in comparison to those from FD and LP. The CP variables occupy ten and

eight places in the first 15 most important variables (including those of the first four and first two) for 2011 and 2014, respectively. In particular, the alpha from the August image was the most important variable in both years, with the largest NVI of 1.26 and 1.01 for 2011 and 2014, respectively. The variables derived from the FD decomposition were of intermediate importance, and they accounted for three and four places in the first 15 most important variables for the 2011 and 2014 classifications, respectively. Among the FD variables, the most important one was the double-bounce scatter from the July image in 2011 and the June image in 2014 (Fig. 6). Moreover, the LP channels were rated as being the least important with only two and three variables squeezed into the first 15 most important places in 2011 and 2014, respectively (Fig. 6).

It is interesting to note that the importance of UAVSAR imagery to the RF classification varied greatly across the time-series dataset. The accumulated normalized importance on a monthly basis over both years with the first 36 most important variables is illustrated in Fig. 7. It can be seen from the figure that the summer acquisitions (June and July in 2011 and June and August in 2014) stand out as possessing the greatest importance, and the spring (May in 2011 and April and May in 2014) and autumn (October in 2011) acquisitions have medium importance values. In contrast, the winter acquisitions (January and December in 2011 and February in 2014) were found to have limited influence on

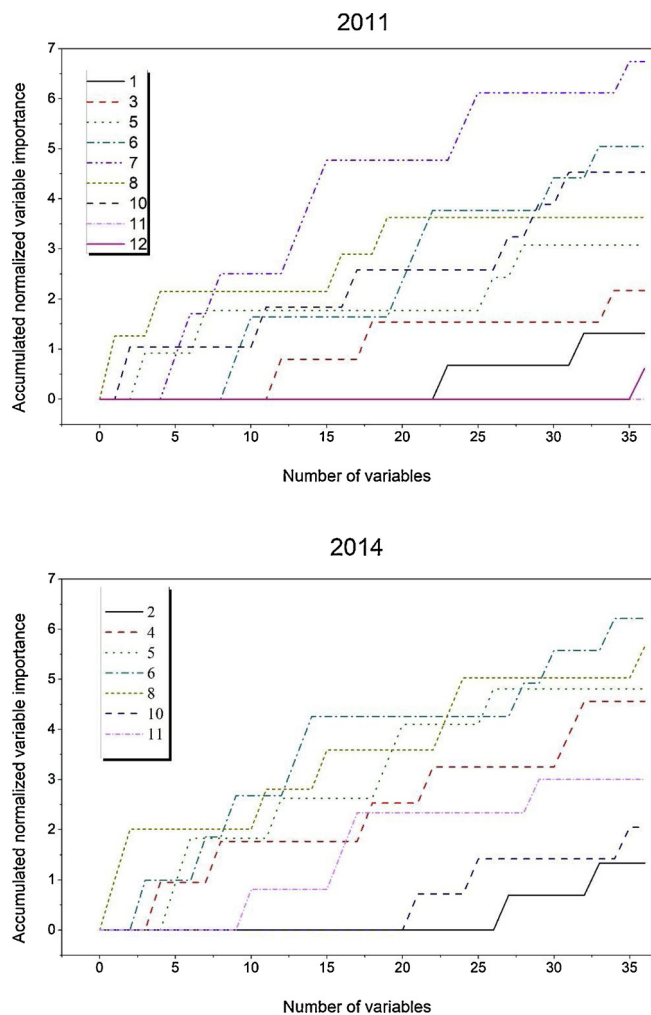


Fig. 7. Histograms of accumulated normalized variable importance from the images dated from January to December. Note that numbers in the legend indicate acquisition dates. For example, “1” denotes the image acquired in January (see Table 1), and so on.

crop classification, and no contribution of importance towards classification was observed for the November acquisition in 2011. In summary, acquisitions during the crop growing season (March to October) are far more important than those during the off season (November to the next March) for the UAVSAR-based crop classification over both of the years (Fig. 7).

4.3. Optimal combination of SAR

The forward image selection results to search for the optimal combination of images (best tradeoff between accuracy and number of images) using the RF for crop classification are shown in Fig. 8. It can be seen from the figure that the August acquisition achieves the highest single date-based overall accuracy (66.23 %) for the year 2011, followed by those dated July, June, and October, while the overall accuracies yielded by the other acquisitions are relatively low. With the adding of images, the overall accuracies first increased rapidly and then became rather stable (Fig. 8). However, the combination of merely four images dated May, July, August, and October produced an early-optimal classification accuracy, with an overall accuracy of 88.26 %. Similarly, for the year 2014 the August acquisition obtained the best single date-based accuracy (64.12 %), and the combination of images dated April, June, August, and October generated an early-optimal classification accuracy of 83.90 %. A Kappa z -test further indicated that

there was no significant difference between the classification based on the four images and that using all images for the year 2011 ($z = 1.62$) and 2014 ($z = 0.60$), respectively. Classification accuracy was not increased substantially when many more images were progressively added to the classifier.

5. Discussion

5.1. Crop classification accuracy

The crop classification accuracies produced in this research were very promising, yielding an overall accuracy of 90.50 % and 84.93 % for 2011 and 2014, respectively, when all predictor variables were available. This is not trivial in consideration of the relatively large number of crop types being considered. The overall accuracy of 2014 was lower than that of 2011 by about 6 percentage points. This is because July UAVSAR image that can make unique contributions to separation of crop types (Li et al., 2019) was not included in the 2014 time-series (Table 1). It should be noted that the classification accuracy might be improved further by applying speckle reduction algorithms to original UAVSAR datasets, as the equivalent number of looks of UAVSAR may markedly increase (Ding et al., 2013). Our results showed that polarimetric parameters outperformed linear polarizations, suggesting that much more valuable information had been provided by the polarimetric parameters. A possible reason for this is that the polarimetric parameters have a close relationship with growth parameters of crops (e.g. plant height, biomass, and leaf area index). However, for the case of dual co-polarized (HH, VV) SAR, polarimetric features (e.g. the correlation coefficient (ρ) and the phase difference (φ) between the co-polarized linear responses), which provide information about the scattering mechanisms (Loosvelt et al., 2012a; Canisius et al., 2018), should be considered for crop classification. In terms of per-class accuracy, we note that accuracies for crop classes with large biomass (tree crops and summer crops) were greater than 91 % and 85 % for 2011 and 2014, respectively, when making use of all variables (Tables 3 and 4). This indicates that L-band microwave with a relatively long wavelength can penetrate into the crop canopy and, thus, capture the unique structural characteristics of those crop types. In contrast, hay and clover, two types of forage crops with relatively small biomass, were classified with mapping accuracies ranging from 63 % to 84 %. Examining the confusion matrix of the classification (not shown in the paper), we found that the mutual mis-identification of the two classes was the main reason for their lower accuracies. For crops with small biomass, surface scattering was overwhelmingly dominant across the full year with L-band images (Li et al., 2019). That is, the unique structural characteristics of small biomass crops are hard to capture due to the effect of soil surface on the radar response, which is responsible for the mutual misclassification of hay and clover in this research. The C-band SAR with a smaller wavelength that observes ground objects at a different scale might be helpful in discriminating these small-biomass crop types (Skriver, 2012).

SAR-based classification accuracy might be affected by weather conditions and incidence angle of radar signal (Skriver et al., 1999). Precipitation may raise soil conductivity and freezing decrease dielectric constant of soil, thus altering the intensity of the backscatter response. Fortunately, nearly all the UAVSAR data over both years used in this work were collected under dry conditions with the minimum air temperatures above freezing point (Table 1), suggesting that weather conditions exerted little impact on crop signatures. The impact of incidence angle is also negligible in this research because of the relatively small area of the test site. Besides, such impact tends to be relatively weak with the growth of crop plants (Saich and Borgeaud, 2000).

5.2. Variable importance of crop classification

The variable importance analysis demonstrated that the

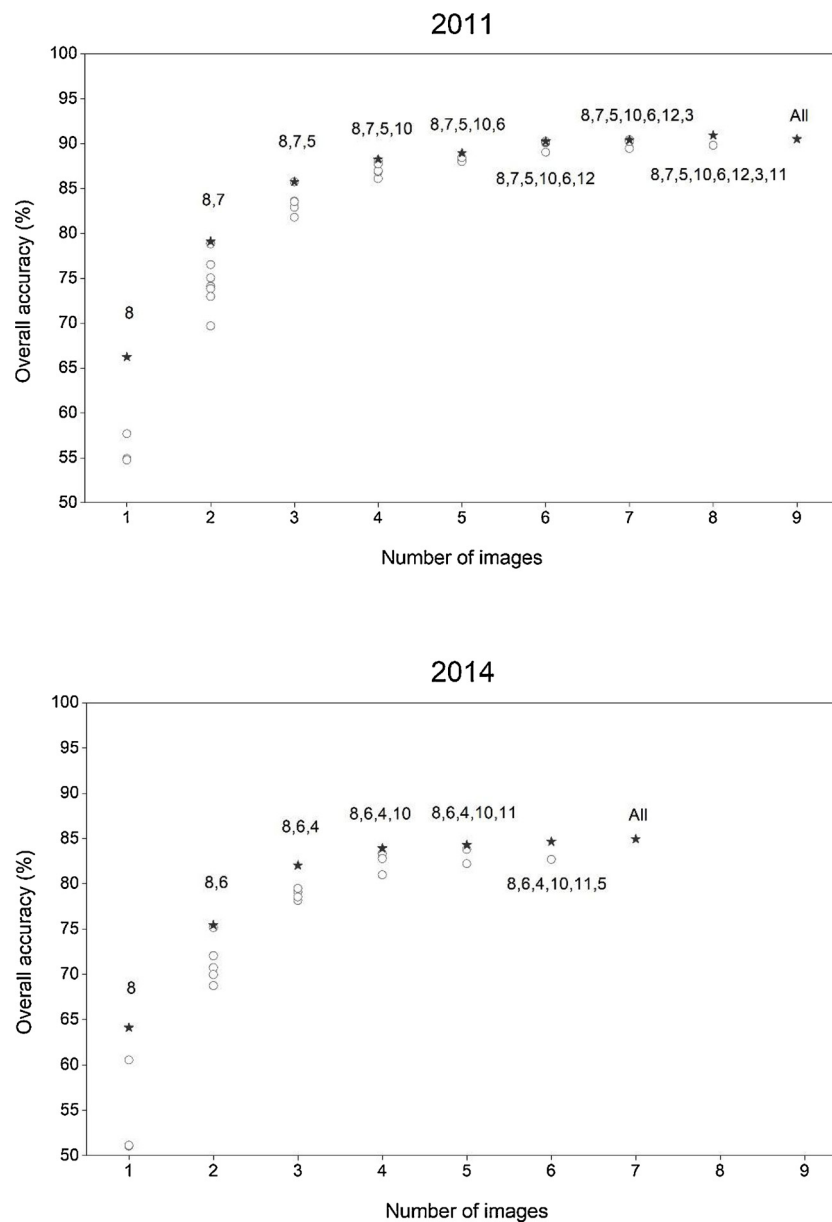


Fig. 8. The RF overall accuracies for the optimal combination of images produced by a forward image selection procedure using all predictor variables. Note that numbers in the figure denote combinations of images, for example “8,7” represents the combination of images dated July and August (see Table 1), and so on.

polarimetric parameters had a far greater influence than linear polarizations, because that with clear physical meanings, these parameters are sensitive to crop biophysical parameters (e.g. Canisius et al., 2018). Moreover, the relatively large value of variable importance achieved by the CP parameters suggested that they were far more important than the FD parameters. This is mainly due to the fact that CP parameters are more sensitive to structural differences between crop types in comparison with the FD parameters (Dickinson et al., 2013). This finding is consistent with a recent study of Canisius et al. (2018), in which a large correlation between plant height and alpha angle (a parameter from CP decomposition) was observed when monitoring the growth of spring wheat and canola using RADARSAT-2 data. It was also found that the importance of UAVSAR imagery to crop classification varied greatly across the year. As expected, images dated during the peak biomass stage (July and August) were the most important, which agrees with our previous JM distance-based research showing that the largest separability amongst crop types occurred during July and August (Li et al., 2019). In contrast, several optical image-based studies reported

that crop types can be best separated during the green-up and senescence phenological stages (e.g. Wardlow et al., 2007; Pena and Brenning, 2015). This might be attributable to the intrinsic differences between optical sensors and SAR. The optical reflectance observed in the visible spectral domain was found to be sensitive to vegetation with low leaf area index (LAI) (Prevot et al., 2003). As a result, crop types can be discriminated with optical images dated during the green-up and senescence stages (Wardlow et al., 2007). In contrast, SAR sensors tend to capture ground targets’ structural characteristics (e.g. height, bulk amount, and texture) which are distinctive amongst crop classes during the peak biomass stage.

5.3. Optimal combination of SAR data

In this research, a combination of only four acquisitions (from May, July, August, and October for 2011 and April, Jun, August, and October for 2014) achieved near-optimal crop classification accuracy. This means that, in addition to the summer acquisitions (June, July, and

August) as mentioned above, images dated during green-up and senescence stages also provided useful information for crop classification. By examining the confusion matrices (not shown here), two fruit crops (almond and walnut) as well as winter wheat and grass were found to be better discriminated from each other when adding the spring acquisitions (May for 2011 and April for 2014) into the image combination. This is mainly attributed to the relatively large difference in canopy structure between almond and walnut as well as winter wheat and grass in spring, resulting from different bloom time (March to mid-April for almond and mid-April to May for walnut) and germination time (last autumn for winter wheat and spring for grass), respectively (Pena-Barragan et al., 2011). Besides, the October acquisition was found to contribute to the separation of corn from the other two summer crops (sunflower and tomato). This is due to the distinctive canopy structure of corn in contrast to sunflower and tomato in Autumn, caused by different harvest time (September–November for corn and July–September for sunflower and tomato) (Li et al., 2019).

6. Summary and conclusion

In this research, the capability of time-series L-band UAVSAR for crop classification was explored using the RF algorithm. The polarimetric parameters from both Cloude–Pottier (CP) and Freeman–Durden (FD) decompositions were superior to linear polarizations with respect to crop discrimination. The synergistic use of all variables further produced an overall accuracy of 90.50 % and 84.93 % for 2011 and 2014, respectively, increasing about 8 percentage points in comparison with those using linear polarizations alone. Polarimetric parameters played a more important role than linear polarizations in crop discrimination, and the CP parameters were found to be much more important than the FD parameters. The most important acquisitions were the images during the peak biomass stage (July and August), and the spring (April and May) and autumn (October) acquisitions were also useful for crop classification as they respectively provided unique information for discriminating fruit crops (almond and walnut) as well as summer crops (corn as well as sunflower and tomato). Hence, a combination of only four images from May, July, August, and October for 2011 and April, June, August, and October for 2014 yielded nearly-optimal classification results, achieving an overall accuracy of 88.26 % and 83.90 %, respectively. Such combinations make the best tradeoff between classification accuracy and number of acquisitions for crop classification.

This research highlights the unique value of multitemporal fully-polarimetric SAR data in crop discrimination over agricultural regions with diverse crop types. The results demonstrate that a relatively high classification accuracy (> 84 %) of agricultural crops can be expected with only a few polarimetric SAR acquisitions. In light of the promising crop classification accuracies acquired in this research, it becomes increasingly viable to attain accurate and up-to-date crops inventories based solely on polarimetric L-band SAR data, which provides a cost-effective alternative to field survey of crops over large areas (e.g. nation-wide scale).

Author statement

Huapeng Li, Ce Zhang, Peter Atkinson: Conceptualization. **Huapeng Li:** Methodology, Software, Validation, Formal analysis, Resources, Data curation, Investigation. **Huapeng Li, Ce Zhang, Shuqing Zhang, Peter Atkinson:** Writing- Original draft. **Huapeng Li, Shuqing Zhang:** Writing- Reviewing and Editing. **Huapeng Li:** Funding acquisition.

Declaration of Competing Interest

We declare no conflict of interest.

Acknowledgements

This research was co-funded by the National Natural Science Foundation of China (41301465), the National Key Research and Development Program of China (2017YFB0503602), and the Jilin Province Science and Technology Development Program (20170520087JH). We thank Alaska Satellite Facility for the supply of UAVSAR data employed in this work.

References

- Bargiel, D., 2017. A new method for crop classification combining time series of radar images and crop phenology information. *Remote Sens. Environ.* 198, 369–383.
- Belgiu, M., Dragut, L., 2016. Random forests in remote sensing: a review of applications and future directions. *ISPRS J. Photogramm. Remote Sens.* 114 (6), 24–31.
- Boryan, C., Yang, Z.W., Mueller, R., Craig, M., 2011. Monitoring US agriculture: the US department of agriculture, national agricultural statistics service, cropland data layer program. *Geocarto Int.* 26 (5), 341–358.
- Breiman, L., 2001. Random forests. *Mach. Learn.* 45 (1), 5–32.
- Canisius, F., Shang, J., Liu, J., Huang, X., Ma, B., Jiao, X., Geng, X., Kovacs, J.M., Walters, D., 2018. Tracking crop phenological development using multi-temporal polarimetric Radarsat-2 data. *Remote Sens. Environ.* 210 (6), 508–518.
- Chapman, B., Hensley, S., Lou, Y., 2011. The JPL UAVSAR. *ASF News Notes* 7 (1) Retrieved from. <https://www.asf.alaska.edu/news-notes/7-1/jpl-uavsar/>.
- Cloude, S.R., Pottier, E., 1997. An entropy based classification scheme for land applications of polarimetric SAR. *IEEE Trans. Geosci. Remote Sens.* 35 (1), 68–78.
- Congalton, R.G., Green, K.G., 1999. Assessing the Accuracy of Remotely Sensed Data: Principles and Practices. Lewis Publishers, Boca Raton, Florida.
- Dickinson, C., Siqueira, P., Clewley, D., Lucas, R., 2013. Classification of forest composition using polarimetric decomposition in multiple landscapes. *Remote Sens. Environ.* 131, 206–214.
- Ding, Z., Zeng, T., Dong, F., Liu, L., Yang, W., Long, T., 2013. An improved PolSAR image speckle reduction algorithm based on structural judgment and hybrid four-component polarimetric decomposition. *IEEE Trans. Geosci. Remote Sens.* 51 (8), 4438–4449.
- Duro, D.C., Franklin, S.E., Dube, M.G., 2012. A comparison of pixel-based and object-based image analysis with selected machine learning algorithms for the classification of agricultural landscapes using SPOT-5 HRG imagery. *Remote Sens. Environ.* 118, 259–272.
- Foody, G.M., 2004. Thematic map comparison: evaluating the statistical significance of differences in classification accuracy. *Photogramm. Eng. Remote Sens.* 70 (5), 627–633.
- Freeman, A., Durden, S.L., 1998. A three-component scattering model for polarimetric SAR data. *IEEE Trans. Geosci. Remote Sens.* 36 (3), 963–973.
- Gislason, P.O., Benediktsson, J.A., Sveinsson, J.R., 2006. Random Forests for land cover classification. *Pattern Recogn. Lett.* 27 (4), 294–300.
- Hensley, S., Zebker, H., Jones, C., Michel, T., Muellerschoen, R., Chapman, B., 2009. First deformation results using the NASA/JPL UAVSAR instrument. In: 2nd Asian-Pacific Conference on Synthetic Aperture Radar. Xi'an Shanxi, China: IEEE. pp. 1051–1055.
- Jiao, X.F., Kovacs, J.M., Shang, J.L., McNairn, H., Walters, D., Ma, B.L., Geng, X.Y., 2014. Object-oriented crop mapping and monitoring using multi-temporal polarimetric RADARSAT-2 data. *ISPRS J. Photogramm. Remote Sens.* 96, 38–46.
- Lee, J.S., Pottier, E., 2009. *Polarimetric Radar Imaging From Basics to Applications*. CRC Press, New York.
- Li, H.P., Zhang, C., Zhang, S.Q., Atkinson, P.M., 2019. Full year crop monitoring and separability assessment with fully-polarimetric L-band UAVSAR: a case study in the Sacramento Valley, California. *Int. J. Appl. Earth Obs. Geoinf.* 74 (02), 45–56.
- Lin, Y.C., Sarabandi, K., 1999. A Monte Carlo coherent scattering model for forest canopies using fractal-generated trees. *IEEE Trans. Geosci. Remote Sens.* 37 (1), 440–451.
- Liu, C., Shang, J.L., Vachon, P.W., McNairn, H., 2013. Multiyear crop monitoring using polarimetric RADARSAT-2 data. *IEEE Trans. Geosci. Remote Sens.* 51 (4), 2227–2240.
- Loosvelt, L., Peters, J., Skriver, H., De Baets, B., Verhoest, N.E., 2012a. Impact of reducing polarimetric sar input on the uncertainty of crop classifications based on the random forests algorithm. *IEEE Trans. Geosci. Remote Sens.* 50 (10), 4185–4200.
- Loosvelt, L., Peters, J., Skriver, H., Lievens, H., Coillie, F.M.B.V., Baets, B.D., Verhoest, N.E.C., 2012b. Random Forests as a tool for estimating uncertainty at pixel-level in SAR image classification. *Int. J. Appl. Earth Obs. Geoinf.* 19, 173–184.
- McNairn, H., Brisco, B., 2004. The application of C-band polarimetric SAR for agriculture: a review. *Can. J. Remote. Sens.* 30 (3), 525–542.
- McNairn, H., Shang, J.L., Jiao, X.F., Champagne, C., 2009. The contribution of ALOS PALSAR multipolarization and polarimetric data to crop classification. *IEEE Trans. Geosci. Remote Sens.* 47 (12), 3981–3992.
- National Oceanic and Atmospheric Administration, National Centers for Environmental Information (NOAA-NCEI), 2011. Local Climatological Data (LCD), Sacramento Executive Airport, Sacramento County, CA. National Environmental Satellite, Data, and Information Service. Retrieved February 3, 2018, from. <https://www.ncdc.noaa.gov/cdo-web/datasets/LCD/stations/WBAN:23232/detail>.
- Ndikumana, E., Minh, D.H.T., Baghdadi, N., Courault, D., Hossard, L., 2018. Deep recurrent neural network for agricultural classification using multitemporal SAR sentinel-1 for camargue, France. *Remote Sens.* 10 (8), 1217.

- Nguyen, D.B., Gruber, A., Wagner, W., 2016. Mapping rice extent and cropping scheme in the Mekong Delta using Sentinel-1A data. *Remote Sens. Lett.* 12 (7), 1209–1218.
- Ozdogan, M., Woodcock, C.E., 2006. Resolution dependent errors in remote sensing of cultivated areas. *Remote Sens. Environ.* 103 (2), 203–217.
- Pena, M.A., Brenning, A., 2015. Assessing fruit-tree crop classification from Landsat-8 time series for the Maipo Valley, Chile. *Remote Sens. Environ.* 171, 234–244.
- Pena-Barragan, J.M., Ngugi, M.K., Plant, R.E., Six, J., 2011. Object-based crop identification using multiple vegetation indices, textural features and crop phenology. *Remote Sens. Environ.* 115 (6), 1301–1316.
- Prevot, L., Chauki, H., Troufleau, D., Weiss, M., Baret, F., Brisson, N., 2003. Assimilating optical and radar data into the STICS crop model for wheat. *Agronomie* 23 (4), 297–303.
- Saich, P., Borgeaud, M., 2000. Interpreting ERS SAR signatures of agricultural crops in Flevoland, 1993-1996. *IEEE Trans. Geosci. Remote Sens.* 38 (2), 651–657.
- Silva, W.F., Rudorff, B.F.T., Formaggio, A.R., Paradella, W.R., Mura, J.C., 2009. Discrimination of agricultural crops in a tropical semi-arid region of Brazil based on L-band polarimetric airborne SAR data. *ISPRS J. Photogramm. Remote Sens.* 64 (5), 458–463.
- Skriver, H., 2012. Crop classification by multi-temporal C- and L-band single and dual polarization, and fully polarimetric SAR. *IEEE Trans. Geosci. Remote Sens.* 50 (6), 2138–2149.
- Skriver, H., Svendsen, M.T., Thomsen, A.G., 1999. Multitemporal C- and L-band polarimetric signatures of crops. *IEEE Trans. Geosci. Remote Sens.* 37 (5), 2413–2429.
- Sonobe, R., Tani, H., Wang, X.F., Kobayashi, N., Shimamura, H., 2014. Random forest classification of crop type using multi-temporal TerraSAR-X dual-polarimetric data. *Remote Sens. Lett.* 5 (2), 157–164.
- Sun, W.X., Liang, S.L., Xu, G., Fang, H.L., Dickinson, R., 2008. Mapping plant functional types from MODIS data using multisource evidential reasoning. *Remote Sens. Environ.* 112 (3), 1010–1024.
- Thenkabail, P.S., Knox, J.W., Ozdogan, M., Gumma, M.K., Congalton, R.G., Wu, Z.T., Milesi, C., Finkral, A., Marshall, M., Mariotto, I., You, S.C., Giri, C., Nagler, P., 2012. Assessing future risks to agricultural productivity, water resources and food security: how can remote sensing help? *Photogram. Eng. Remote Sens.* 78 (8), 773–782.
- Thornton, P.K., Bowen, W.T., Ravelo, A.C., Wilkens, P.W., Farmer, G., Brock, J., Brink, J.E., 1997. Estimating millet production for famine early warning: an application of crop simulation modelling using satellite and ground-based data in Burkina Faso. *Agric. For. Meteorol.* 83 (1–2), 95–112.
- Tso, B., Mather, P.M., 1999. Crop discrimination using multi-temporal SAR imagery. *Int. J. Remote Sens.* 20 (12), 2443–2460.
- Wang, D., Lin, H., Chen, J., Zhang, Y., 2010. Application of multi-temporal ENVISAT ASAR data to agricultural area mapping in the Pearl River Delta. *Int. J. Remote Sens.* 31 (6), 1555–1572.
- Wardlow, B.D., Egbert, S.L., 2008. Large-area crop mapping using time-series MODIS 250 m NDVI data: an assessment for the US Central Great Plains. *Remote Sens. Environ.* 112 (3), 1096–1116.
- Wardlow, B.D., Egbert, S.L., Kastens, J.H., 2007. Analysis of time-series MODIS 250 m vegetation index data for crop classification in the US Central Great Plains. *Remote Sens. Environ.* 108 (3), 290–310.
- Whelen, T., Siqueira, P., 2017. Use of time-series L-band UAVSAR data for the classification of agricultural fields in the San Joaquin Valley. *Remote Sens. Environ.* 193, 216–224.
- Zheng, B.J., Myint, S.W., Thenkabail, P.S., Aggarwal, R.M., 2015. A support vector machine to identify irrigated crop types using time-series Landsat NDVI data. *Int. J. Appl. Earth Obs. Geoinf.* 34, 103–112.
- Zhong, L.H., Gong, P., Biging, G.S., 2012. Phenology-based crop classification algorithm and its implications on agricultural water use assessments in California's central valley. *Photogram. Eng. Remote Sens.* 78 (8), 799–813.